

Highlights

A Fully Automated and Scalable Surface Water Mapping with Topographic Airborne LiDAR Data

Hunsoo Song, Jinha Jung

- We present an automated and scalable surface water mapping method.
- Our method extracts surface water based on the natural law that surface water is flat.
- Our method is particularly advantageous in steep mountains and urban areas with very small water bodies.
- Our method enables a full 3D topography mapping using only airborne LiDAR data.

A Fully Automated and Scalable Surface Water Mapping with Topographic Airborne LiDAR Data

Hunsoo Song^a, Jinha Jung^{a,*}

^aThe Lyles School of Civil Engineering, Purdue University, 550 Stadium Mall Drive, West Lafayette, Indiana, the United States

ARTICLE INFO

Keywords:

Surface water mapping
Airborne LiDAR data
Region merging
Small water bodies

ABSTRACT

Reliable and accurate high-resolution maps of surface waters are critical inputs to models that help understand the impacts and relationships between the environment and human activities. Advances in remote sensing technology have opened up the possibility of mapping very small bodies of water that are closely related to people's daily lives and are mostly affected by anthropogenic pressures. However, a robust and scalable method that works well for all types of water bodies located in diverse landscapes at high-resolution has yet to be developed. This paper presents a method that can accurately extract surface water bodies up to a very fine scale in a wide variety of landscapes. Unlike optical image-based methods, the proposed method exploits the robust assumption that surface water is flat as gravity always pulls liquid molecules down. Based on this natural law, the proposed method extracts accurate, high-resolution water bodies including their elevations in a fully automated manner using only airborne LiDAR data. Extensive experiments with large ($\approx 2,500\text{km}^2$) and diverse landscapes (urban, coastal, and mountainous areas) confirmed that our method can generate accurate results without site-specific parameter tunings for varied types of surface water. The proposed method enables an automated, scalable high-resolution mapping of a full 3D topography that includes both water and terrain, using only point clouds for the first time. We will release the code to the public in the hope that our work would lead to more effective solutions to help build a sustainable and resilient environment.

1. Introduction

Surface water maps provide important knowledge to help understand the impacts and relationships between the environment and human activities. Knowing where water is and how it changes and relates to the surrounding environment enables successful responses that are closely related to water resources (Poff et al., 2016; Viviroli et al., 2011; Flörke et al., 2018), biodiversity (Cawse-Nicholson et al., 2021), and human well-being (Sanders et al., 2022).

Optical remote sensing technology has become the most widely adopted and powerful tool for surface water mapping (Huang et al., 2018). Standard practice for extracting water using optical imaging is to exploit the spectral characteristics of water that the reflectance of water is significantly lower in the infrared channel than other channels compared to other objects (Xu, 2006; Ji et al., 2009). Large bodies of water, such as oceans, rivers, and lakes, have been the focus of water mappings since early Earth observation satellite missions (Pekel et al., 2016; Khandelwal et al., 2017), and reflectance-based water mapping has shown successful performance on medium- and low-resolution ($>100\text{m}$) satellite imagery (Feyisa et al., 2014; Yamazaki et al., 2015).

With the development of high-resolution imaging technology, mapping of very small water bodies ($<1\text{ha}$ or $10,000\text{m}^2$) also become possible. Particularly, as small water bodies, such as small lakes, ponds, low-level streams, and ditches, are closely related to people's daily lives and are highly affected by anthropogenic footprints, the demand for a very

high-resolution map of water bodies has been rapidly increasing these days (Kelly-Quinn et al., 2022; Xu et al., 2020; Hoekstra et al., 2018; Biggs et al., 2017; Riley et al., 2018). However, in high-resolution images, conventional reflectance-based water mapping does not show satisfactory performance (Ogilvie et al., 2018) and often underestimates the extent of small water bodies (Pickens et al., 2020; Mao et al., 2022). This is mainly because the reflectance of small water bodies is highly varying in high-resolution images while high-resolution images require multiple image acquisitions to cover large-area which will again significantly increase the spectral variability.

To address this problem, efforts have been made to develop more sophisticated methods. Integrating multi-temporal (Pickens et al., 2020) or different types of sensors (e.g., radar) (Ahmad et al., 2019) or developing data-driven methods (Ko et al., 2015; Isikdogan et al., 2017; Chen et al., 2020; Wang et al., 2020) are examples. However, fundamentally, algorithms based on optical images cannot be free from spectral characteristics of water whose values vary depending on image acquisition conditions e.g., atmospheric conditions and sensor specifications (Martins et al., 2017) or surface water conditions (e.g., turbidity and surface roughness) (Odermatt et al., 2012; Kim et al., 2016).

In addition, current optical image-based water mapping algorithms are limited to providing only 2D information. Meanwhile, even simply for identifying the direction of water flow, 3D topographic information is needed. Obviously, 3D water information can provide better information for understanding the dynamics of water, and it enables in-depth analysis of how water relates to its surrounding environments and improves the management of water resources and water-related

*Corresponding author

✉ hunsoo@purdue.edu (H. Song); jinha@purdue.edu (J. Jung)

ORCID(s): 0000-0001-6899-6770 (H. Song); 0000-0003-1176-3540 (J. Jung)

Jung)

disasters (Musa et al., 2015; Jarihani et al., 2015; Arrighi and Campo, 2019). Thus, the authors note that airborne laser scanning will eventually be required for surface water maps to be truly useful as the LiDAR data is needed to obtain high-resolution 3D topographic information. Nevertheless, as airborne laser scanning has not been effectively used for surface water mapping, separate resources and efforts have been required for completing a 3D hydrography.

This paper presents a scalable water mapping method using topographic airborne LiDAR data. The scalable method refers to the method that yields consistently satisfactory results across wide and varied landscapes. Our method operates in a fully automated manner, only requires topographic airborne LiDAR data, and extracts accurate and high-resolution water bodies including the elevation of water bodies. Extensive experiments with large ($\approx 2,500\text{km}^2$) and diverse landscapes (urban, coastal, and mountainous areas) confirmed that our algorithm can generate more accurate results than NDWI-based methods even without any additional parameter tunings. Moreover, the proposed method enables high-resolution mapping of a full 3D topographic map (water and terrain) with only airborne LiDAR data.

The remainder of this paper is organized as follows. Section 2 illustrates related works. Section 3 describes the proposed surface water mapping methods. Section 4 illustrates datasets and experimental design. Section 5 provides experimental results. Section 6 concludes the paper.

2. Related works

2.1. Optical imagery-based water mapping

Optical imagery has been dominantly used for surface water mapping. With multiple satellite missions at different spatial resolutions ranging from 1 km to 1-m resolution, water bodies of the Earth have been mapped for more than several decades (Pekel et al., 2016; Khandelwal et al., 2017). In particular, with recent advancements in satellite, airborne, and UAV imaging technology, a large-area mapping of small water bodies has attracted more attention (Becker et al., 2019; Straffellini et al., 2021; Qayyum et al., 2020; Sogno et al., 2022).

Although the higher spatial resolution imagery enables observing small water bodies, large-area mapping of small water bodies is more complicated than that with the lower resolution imageries for large water bodies. This is because, first, small water bodies have more wide variety of spectral reflectance (Ogilvie et al., 2018). Second, shadow, occlusion, and relief displacement of urban structures make water mapping more challenging (Yang et al., 2018). Third, large-area mapping with high-resolution imagery necessitates multiple different image acquisitions, while different acquisitions may require different threshold values for water index-based mapping (Feyisa et al., 2014).

To improve the accuracy, some recent studies have developed more sophisticated decision rules. (Yang et al., 2018) alleviated errors from built-up areas by utilizing multiple water and shadow indices. (Dong et al., 2022) integrated

the spatial information into the classification rule by introducing the roughness of the water index. In addition, there have been studies that used data-driven approaches such as support vector machine (Sun et al., 2015), random forest (Ko et al., 2015), and deep learning methods (Chen et al., 2020; Isikdogan et al., 2017; Wang et al., 2020).

More often, water has been mapped with other multiple classes including ice and cloud (Wu et al., 2018) or more comprehensive land covers (Song et al., 2019; Robinson et al., 2019; Zhang et al., 2022). Most methods obtained satisfactory results under the condition that sufficient high-quality training samples are available. However, acquiring high-quality training samples for large areas is a challenging task, particularly in high-resolution image, for the same reason that surface water mapping using spectral characteristics is difficult (Pickens et al. (2020); Liu et al. (2021); Murray et al. (2022)). Moreover, the decision rule of data-driven approaches is generally not clear and their results are biased towards the training data distribution (Moreno-Torres et al., 2012), which makes quality control of their output difficult.

2.2. Airborne LiDAR based water mapping

Relatively very few studies have used topography airborne laser scanning for surface water mapping. Topographic airborne laser scanning refers to the system operated with the near infrared laser. We exclude bathymetry LiDAR in our discussion. The main idea of surface water mapping with LiDAR is to take advantage of the intensity values of airborne LiDAR and the property that the point density of LiDAR point clouds within water areas is much lower than in non-water areas as water hardly reflects the laser point.

(Brzank et al., 2008) performed a supervised fuzzy classification using using height, intensity, and point density as input. (Höfle et al., 2009) modeled both intensity and point density based on the sensing geometry and performed a seeded region growing segmentation and object-based classification for surface water mapping. (Smeeckaert et al., 2013) used a support vector machine for water extraction based on historical coastline data. This study refined the coastline data and conducted a supervised classification using 3D point-based features. (Crasto et al., 2015) performed a decision tree-based data-driven approach using point density, elevation, and intensity of LiDAR points as inputs. More recently, (Malinowski et al., 2016) input radiometric and geometric laser point features of full-waveform LiDAR into supervised classifiers to conduct flood mapping. (Shaker et al., 2019) input multispectral LiDAR-based features into the log-likelihood classification model and performed supervised classification for water mapping. Also, (Yan et al., 2019) performed water body mapping by developing a method that collects training samples based on the ratio of intensity and elevation for each scan line and performs a classification using the maximum likelihood model.

To sum up, state-of-the-arts LiDAR-based water mapping methods exploit the properties of water which are characterized by the low intensity and low point density over water bodies. Also, many studies tried to calibrate the intensity

values. However, intensity values are easily confounded by many other factors such as sensor orientation, scan angles, and turbidity and roughness of water surfaces, which require even more concrete calibration than that for the optical images. In the end, LiDAR-based water mapping methods end up relying on data-driven approaches which require human interventions and high-quality training data; while the performance of data-driven approaches highly depends on the quality of training data and is susceptible to data distribution shifts, just like the case of optical image-based methods.

2.3. Limitations and opportunities

A major barrier to developing scalable water body mapping in both optical and LiDAR-based methods has been an inconsistent spectral characteristic of water in remote sensing data (reflectance in optical imagery; intensity in airborne LiDAR). This problem becomes more challenging in high-resolution image, it will involve many more small water bodies whose spectral properties are more diverse and more influenced by the surrounding environment. In addition, large-area mapping requires multiple image acquisitions because individual swath width is limited, especially in high spatial resolution imaging; while multiple image acquisitions increase the likelihood of involving different atmospheric conditions or may involve different types of sensors, which will eventually make scalable water mapping much more difficult.

In the meantime, topography is defined by terrain and water, and they interact and determine each other's shape. For the complete topography mapping, both terrain and water maps are needed. In addition, as discussed, we need a three-dimensional terrain to make surface water map truly impactful. This is why airborne laser scanning is necessary for the high-resolution 3D hydrography mapping. National-scale airborne LiDAR data has been widely collected nowadays. It gives us a great opportunity for large-area mapping at high-resolution. However, since the performance of water mapping using LiDAR is not as effective as using optical imagery, airborne LiDAR data has been used only for terrain mapping and has not been effectively used for water mapping.

In this paper, we developed a scalable water mapping workflow that only requires topographic airborne LiDAR data. The workflow uses only the 3D coordinates of the earth and leverages the geometric and signal properties of water from topographic airborne LiDAR data. As the intensity data is not used, any sensor-specific calibration is not needed, and uncertainties from spectral variability can be avoided. Our workflow extracts water segments based on the LiDAR's point density and extends the extent of each segment based on the robust assumption that the local surface water is flat. With the proposed method, it is now possible to obtain full 3D topographic map in a fully automated manner.

3. Proposed water mapping method

3.1. Overall strategy

A standard LiDAR sensor for topographic scanning emits near-infrared laser pulses whose most of the energy is absorbed by the water or specularly reflected away from the receiver's field of view. Therefore, water bodies can be characterized by a large number of laser point dropouts in topographic airborne LiDAR data. In other words, local point density of LiDAR point clouds can be a variable that distinguishes water from non-water. However, the tricky part is that even within the same water body, local point densities can vary greatly, and there are non-water regions where the local point density is lower than that of a water body due to occlusion. The main reason for the point density variability within water body is varying incidence angle. Theoretically, the number of recorded laser points should gradually decrease as incidence angle increase. However, not only the surface conditions on the ground and water, but also the sensor orientation due to the physical movement of the airborne platform greatly influences the local point density over the surface. To overcome the limitation of solely relying on point density, previous studies have utilized intensity information. However, intensity values are also greatly affected by sensing conditions, which could make scalable water body mapping more difficult.

The proposed method simply uses only 3D coordinate information of point clouds. It does not use the intensity information. Instead, we add an assumption that local surface water is flat. This assumption is robust as the way of water is always downwards and locally connected. Figure 1 shows a pictorial example of typical airborne laser scanning. The red dot represents points that are reflected and observed by the receiver. Only red dots' 3D coordinates are the input of the proposed method. As shown, low point density can either indicate a water body or an occluded area by buildings. Therefore, the proposed method first considers the area with low point density as the initial water segment but excludes the false water segment caused by occlusion of high-rise buildings. On the other hand, some regions of the water body can have as a high point density as the ground due to the low incidence angle, which makes the initial water segment not comprehensive. Thus, the proposed method extends the initial water segment using the water elevation-based region

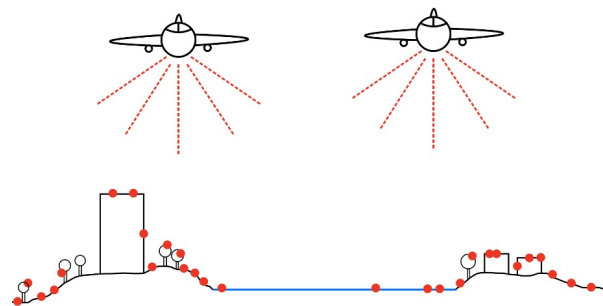


Figure 1: Profile view of an airborne laser scanning

merging. Specifically, the proposed method extends the initial water segment by merging other water segments whose elevations are the same as the initial water segment and that are connected to the initial segment at the same time. To sum up, the proposed method consists of the following two steps (1) initial water segment extraction, and (2) water elevation-based region merging (WERM).

3.2. Initial water segments extraction

In the proposed method, initial water segments are extracted based on the assumption that the point density over water bodies is much lower than in non-water areas as water bodies hardly reflect laser points. Please refer to “1. Water segments extraction” of Figure 2.

First, the proposed method rasterized the raw airborne LiDAR data into a high-resolution 2D gridded space, digital surface model (DSM). If the point clouds are rasterized into high-resolution 2D gridded space, there will be pixels where any laser point is not registered, and areas with more non-registered pixels are more likely to be water bodies. Our method calculates the average point density (P) of a DSM by dividing the number of non-empty cells by the number of total cells. Then, the number of non-empty cells in a certain size of a sliding window (N_{pixels}) will have a binomial distribution $B(N, P)$. Specifically, $B(N, P/2)$ was used to compensate for the imbalance of point density due to scanning overlap and to avoid overly detecting water. Based on the binomial distribution, a lower confidence bound was used for the decision boundary of the water classification. Simply put, the center of sliding window will be classified as a water pixel if the sliding window contains relatively fewer numbers of laser points than other windows.

As a default, we rasterized the point clouds into a 0.5-meter resolution grid, and we used a window of 9 x 9 and a confidence level value of 2 (the critical z-score) as a default. In addition, as shown in Figure 1, as lower local point density can be due to an occlusion from adjacent high-rise buildings, the proposed method adopts a 3D building mapping algorithm (Song and Jung, 2022b) as an optional operation to exclude false positives by creating a building buffer. This operation is only for urban areas with high-rise buildings, as non-urban areas rarely have occlusion large enough to be extracted by water.

3.3. Water Elevation-based Region Merging (WERM)

As the initial water segment is not comprehensive, the proposed method extends the initial water segment based on the assumption that the elevation of the connected water segment is the same. Please refer to “2. Water Elevation-based Region Merging (WERM)” in Figure 2.

First, for each initial water segment, regions of the same elevation are extracted by slicing the DSM based on the elevation. Then, if any extracted region is connected to the initial water segment, the region is merged into the initial water body. In this way, the algorithm WERM expands initial water segments to neighboring regions whose elevations

are very close to each initial water segment. Finally, all initial water segments and the merged water segment will be the final surface water map.

Specifically, in WERM, we picked the 10th percentile of elevations of each initial water segment as the elevation of the water segment. As a default, WERM finds regions of the same elevation by slicing the DSM within $\pm 0.1m$ elevation range considering the vertical precision of airborne LiDAR data. Of all initial segments of water, WERM only works for bodies of water larger than $500m^2$ to exclude insignificant water bodies such as small pools and puddles. Lastly, WERM runs twice as the extended water segment after the first run can give a more reliable elevation value of each segment. The default numerical values (10th percentile, $\pm 0.1m$, and $500m^2$) used in WERM are empirically determined and can be modified. A more detailed discussion in parameter values can be found in Section 6.

4. Datasets and experimental design

Extensive and various landscapes were used for the evaluation as the development of a scalable water mapping algorithm is our goal. Five different large-scale datasets were employed for the evaluation (Figure 3). The five datasets include three metropolitan areas, one mountainous area, and one coastal area. Seas, lakes, rivers, streams, ponds, wetlands, ditches, and snows were included in the dataset. Approximately $2,500km^2$ area, 10 billion pixels evaluated at 0.5-meter resolution.

For the quantitative evaluation, we employed the water body layer of the USGS’s High Resolution National Hydrography Dataset Plus (NHDPlus HR) Moore and Dewald (2016); Moore et al. (2019). NHDPlus HR is an integrated set of geospatial data layers, including the best available National Hydrography Dataset (NHD) and the National Watershed Boundary Dataset (WBD). Also, we compared the proposed method to NDWI-based thresholding methods.

Specifically, we used two different NDWI-based methods that have different levels of privileges. For the first method, we found a single optimal threshold value that makes the method obtain the highest possible overall accuracy compared to the ground truth (NHDPlus HR) for each experimental area. For the second method, we divided each dataset into small-sized tiles and found the optimal threshold value for every individual small-sized tile. Thus, the first method (“NDWI-G-Opt”) creates a surface water map using the global optimal threshold value; while the second method (“NDWI-L-Opt”) creates a surface water map that is stitched with small-sized tiles that are locally optimized to obtain the highest performance for each tile. Although the two NDWI-based methods are not feasible in real practice as the groundtruth must be unknown, we used them to evaluate the proposed method’s performance with more competitive criteria. On the other hand, for the proposed method, we used the same parameter values for the entire dataset. No site-specific optimization was carried out. In this way, we investigate the scalability and the performance of the proposed method in comparison with highly competitive NDWI-based methods

Water Mapping Workflow

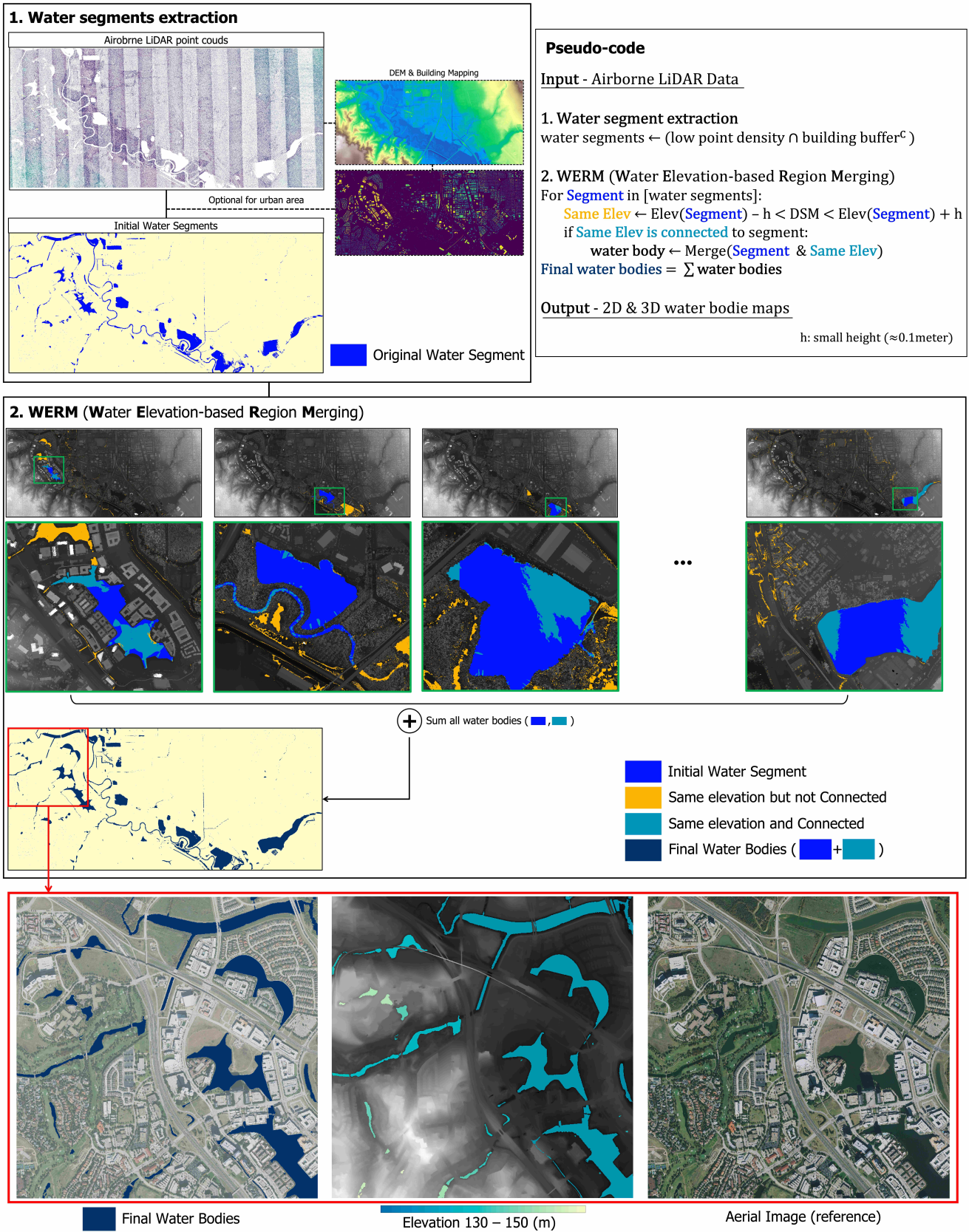


Figure 2: A graphical illustration of the proposed method

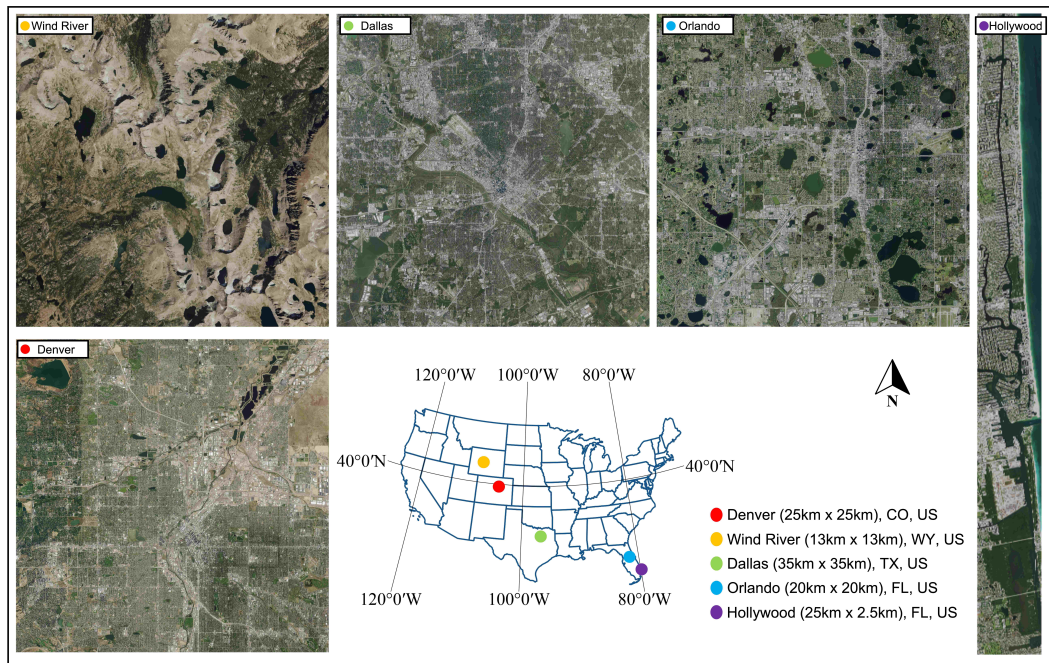


Figure 3: Five large-area datasets over the US: Denver, Wind River, Dallas, Orlando, and Hollywood

Table 1
Summary of the experimental datasets

Name	Denver	Wind River	Dallas	Orlando	Hollywood
Location	Denver, CO	Wind River, WY	Dallas, TX	Orlando, FL	Hollywood, FL
Dimension	25-km by 25-km	13-km by 13-km	35-km by 35-km	20-km by 20-km	25-km by 2.5-km
Geography	Metropolitan area	Mountainous area	Metropolitan area	Metropolitan area	Coastal area
Scanning details	Leica TerrianMapper 2.4 points/ m^2	Leica TerrianMapper 2.0 points/ m^2	Leica ALS 80 3.0 points/ m^2	Leica ALS 80 9.8 points/ m^2	Riegl VG-1560i 8.2 points/ m^2
	AGL: 2.7-3.1km scan angle: 40° overlap: 20%	AGL: 3.0-3.2km scan angle: 40° overlap: 25%	AGL: 1.8km scan angle: 35° overlap: 30%	AGL: 1.4km scan angle: 40° overlap: 60%	AGL: 1.3km scan angle: 60° overlap: 30%
	Terrain elevation	25-km by 25-km	13-km by 13-km	35-km by 35-km	20-km by 20-km
LiDAR acquisition	2020.05.-2020.06.	2019.08.-2019.09.	2019.03.-2019.07.	2018.12.-2019.03.	2018.06.
NAIP acquisition	2019.08.-2019.09.	2019.08.	2020.10.-2020.11.	2019.11.	2019.11.

to which we have given special benefits.

Table 1 summarizes the five datasets. Not only geographic diversity but also diversity of laser scanning conditions are taken into account for the assessment. All airborne LiDAR data were from the USGS's 3D Elevation Program (3DEP) (<https://www.usgs.gov/3d-elevation-program>) Stoker and Miller (2022). For the NDWI-based water mapping, near infrared and green bands of the National Agriculture Imagery Program's optical imagery (NAIP) was used.

The experimental dataset is very large. Providing averaged quantitative results for all datasets might be not sufficient to investigate the performance in-depth. Also, NHD plus datasets include snows, wetlands, and some mangroves as water class while the proposed method and NDWI-based method are intended to extract only surface water bodies.

To address these issues, tile-based evaluation was introduced in addition to the conventional quantitative evaluation to conduct more detailed evaluations in various ways. The tile-based evaluation method proceeds as follows. First, the entire experimental area was divided into small-sized tiles. Then, quantitative evaluation was conducted after excluding tiles that have significant amounts of wetlands and snow cover. In addition, we performed a separate evaluation for only selected challenging tiles based on the magnitude of disagreements among surface water maps. To be specific, we calculated a tile-based difference in intersection over unions (IoU) of the proposed method and the NDWI-based method. Then, we selected challenging areas based on the tile-based IoU difference. Lastly, we selected three sets of tiles for each dataset and investigated the difference both

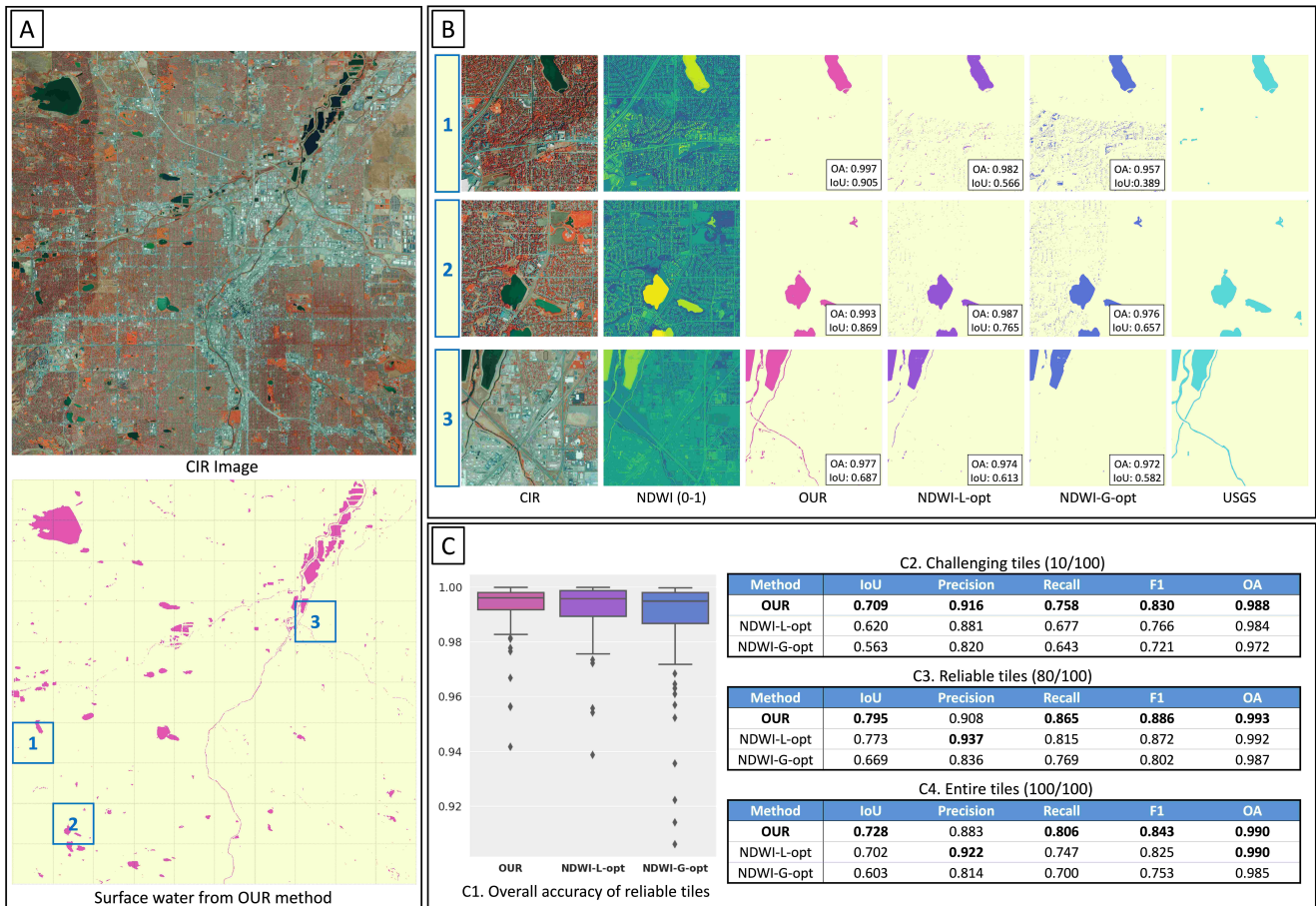


Figure 4: Results of the Denver dataset

quantitatively and qualitatively. In this way, we tried to evaluate the performance of the proposed algorithm effectively and objectively in extensive datasets.

5. Experimental results

Figure 4 shows the results for the Denver dataset. Figure 4-A shows the CIR image and extracted surface water map from the proposed method for the entire Denver dataset. OUR represents surface water maps generated from the proposed method. Figure 4-B highlighted three subset regions that showed significantly different results. CIR, NDWI, and four different surface water maps were visualized. Overall accuracy (OA) and IoU compared to USGS's surface water map were also noted. Figure 4-C shows the statistics of the three methods. C1 boxplot displays the overall accuracies of the three methods. C2, C3, and C4 show the comparison results for three different sampled sets. C2 shows the results from the top 10 challenging tiles that showed the largest IoU difference among different methods. C3 shows the results after excluding tiles whose groundtruths contain significant amounts of snow or wetland cover. Lastly, C4 shows the results from the entire tiles of the Denver dataset.

As shown in Figure 4-A, it is confirmed that the visually identifiable large water bodies are generally well-extracted.

The entire 25-km by 25-km test area was divided into 100 square tiles, of which the tile showing the largest difference were enlarged and displayed in Figure 4-B. As shown in the first row of Figure 4-B, the proposed method hardly generated false positives in the urban area compared to the other two NDWI-based methods. NDWI-L-opt used the locally optimized threshold to obtain the highest possible OA in the given tile. Even though it is tuned using the USGS's water map, there are a large amount of spurious false positives in the urban area. NDWI-G-opt was able to detect some water bodies that were not extracted in NDWI-L-opt, but more false positives were detected in the urban area, resulting in lower OA and IoU.

Similarly, in the second row of Figure 4-B, the proposed method accurately extracted water bodies. However, NDWI-L-opt failed to detect some water bodies; while NDWI-G-opt generated too many false positives. Lastly, in the third row, the proposed method showed very similar results to the USGS water body. A closer look at the stream in the upper left shows that the proposed method can depict the detailed branches of the stream in more detail than the body of water in the USGS. On the other hand, the two NDWI-based methods were not able to accurately detect streams. If the NDWI threshold had been set to a lower value, the NDWI-based method would have been able to detect the stream, but

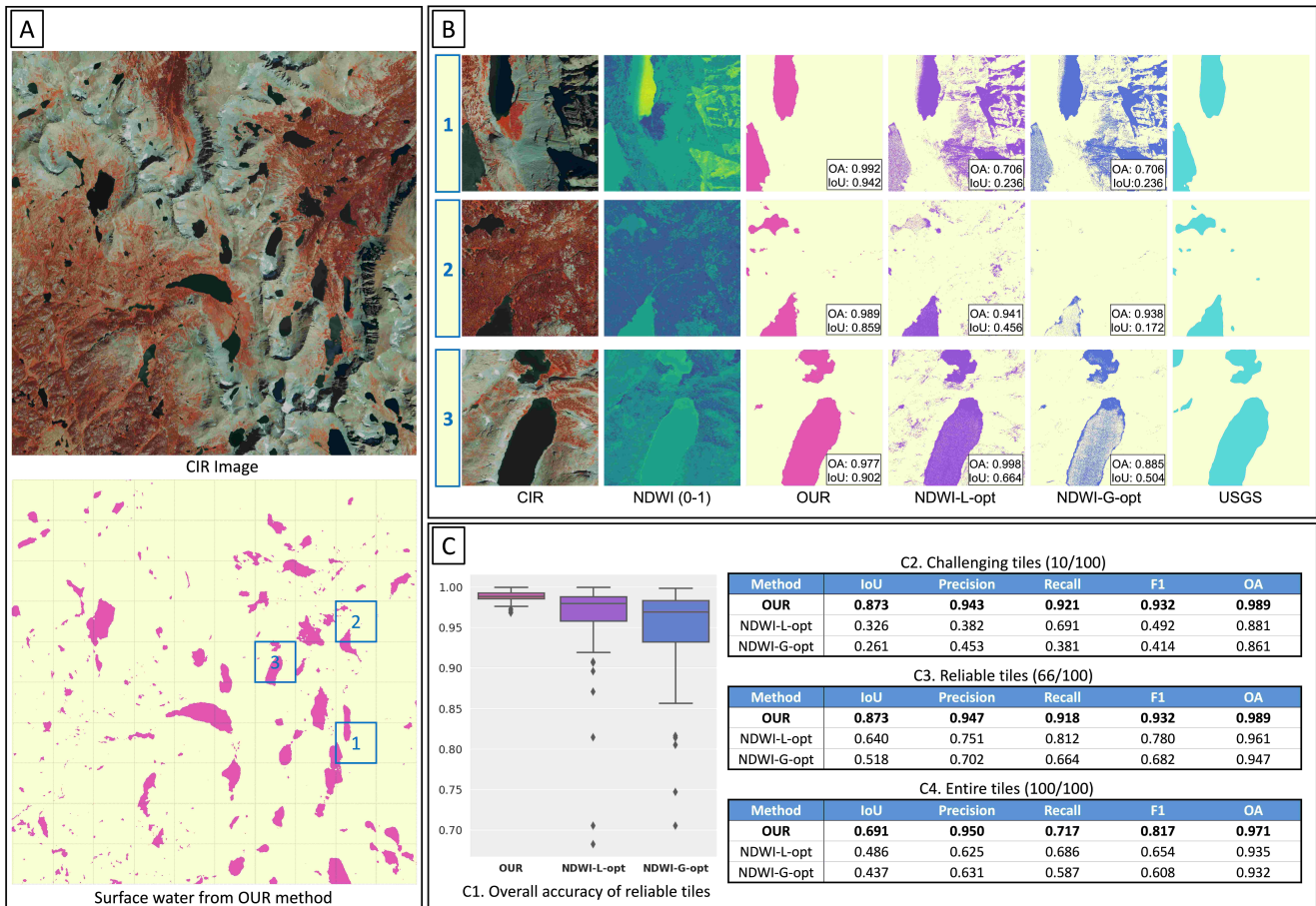


Figure 5: Results of the Wind River dataset

false positives would have increased significantly.

As shown in boxplot C1 in Figure 4, overall accuracies are not significantly different although the proposed method has the least deviation overall. C2 shows the quantitative result by selecting only the top 10 tiles with the largest difference in IoU value among all 100 tiles. The proposed method recorded the highest accuracy in all metrics. The recall was particularly higher than other methods, indicating that the proposed method can achieve a high detection rate in small water bodies such as streams, as confirmed in the third row of Figure 4-B. The following C3 is the evaluation result using the filtered groundtruth, excluding 20 tiles that have a fairly large error in the water map of the USGS. Lastly, C4 is the evaluation result using the entire 100 tiles without filtering any tiles. In both C3 and C4, the proposed method recorded higher accuracies than NDWI-based methods overall. NDWI-L-opt obtained the highest precision. This is partly because NDWI-L-opt is tuned to get the highest OA for each tile, which makes NDWI-L-opt tend to map water bodies passively and avoid false positives.

Figure 5 shows the experimental results of the Wind River dataset. Similar to the layout in Figure 4, Figure 5-A shows the CIR image and the surface water map generated by the proposed method for the entire area, Figure 5-B shows three subset regions, and Figure 5-C shows the statistics of the ex-

periment results.

As can be seen in Figure 5-A, the Wind River dataset is a completely mountainous terrain with no man-made structures, and steep and rugged terrains cast many shadows. Seeing the surface water map generated by the proposed method, it can be confirmed that the proposed method distinguishes between water areas and shadow areas that are difficult to distinguish visually.

Figure 5-B selects and shows three areas where there is a large difference in accuracy between water extraction methods. As shown in the first row, the proposed method clearly distinguishes the water body and the shadow caused by the terrain and records very high accuracy, but the method using the NDWI fails to distinguish between water and shadow despite applying an optimal threshold. In the NDWI-based methods, there were noises in the areas shaded by rugged terrain and trees as shown in the second and third rows. On the other hand, the proposed method generally showed very similar results to USGS and recorded very high accuracy. One error in the upper left corner of the third row was due to the snow cover.

As shown in boxplot C1 in Figure 5, the proposed method recorded higher OAs in general, and its variation was also very low. On the other hand, the NDWI-based method recorded significantly lower OA. Moreover, for all quantitative met-

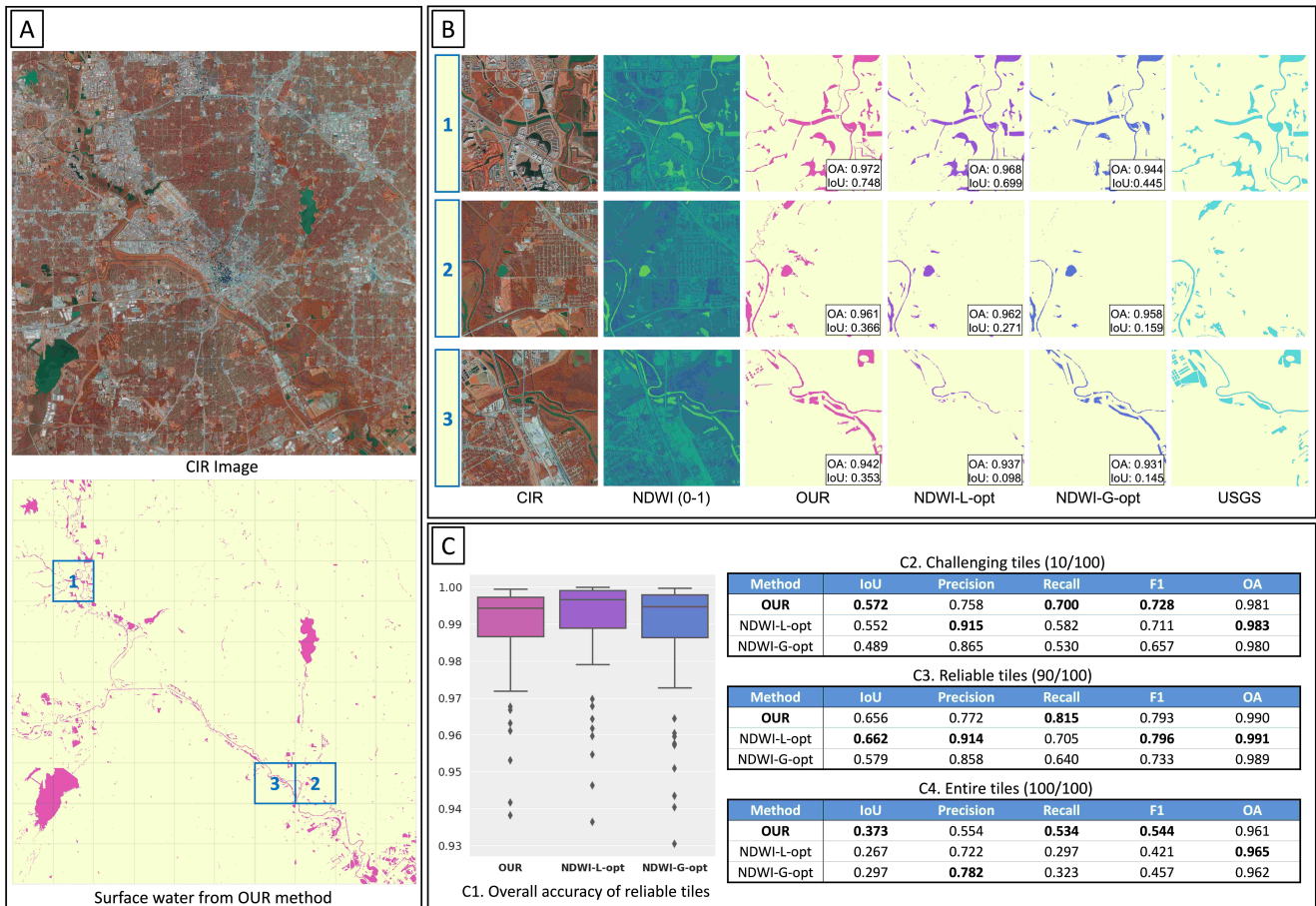


Figure 6: Results of the Dallas dataset

rics in C2–C4, our proposed algorithm recorded significantly higher accuracy than NDWI-based methods.

The Dallas dataset is a 35-km by 35-km metropolitan area covering various types of water bodies. Including several large lakes, the Trinity River and streams branching off from it are widely distributed. There are also many small wetlands, streams, and ponds throughout.

Figure 6-B shows three sampled areas that show significant differences among surface water maps. The first row shows the reservoirs, streams, and lakes of the urban area. The proposed method recorded the highest values in both OA and IoU, and when visually compared with the USGS water body, the water body layer generated by the proposed method showed little error. Rather, small creeks that were not extracted in USGS were well detected by the proposed method. Meanwhile, NDWI-L-opt and NDWI-G-opt were not able to extract water bodies as well as the proposed method. In particular, NDWI-G-opt had lots of omission errors. Considering that NDWI-G-opt used a single threshold for the entire area to yield the highest OA, the result indicates that a single fixed threshold for large areas cannot guarantee satisfactory performance. In the second row of Figure 6-B, NDWI-L-opt recorded the highest overall accuracy. However, it was found that the USGS water layer has some errors probably due to the temporal discrepancy. When com-

pared to the CIR image, the proposed method extracted small creeks well; while the two NDWI-based methods failed to detect creeks successfully. This sample shows an example that differences in quantitative metrics do not accurately represent actual performance. A similar result was also confirmed in the third row of Figure 6-B.

As shown in Figure 6-C, the overall performance of the proposed method was quite similar to that of NDWI-L-opt. In general, the proposed method tends to detect more water, considering the high recall and low precision. This might be attributed to the fact that the proposed method detects small water bodies more comprehensively as shown in Figure 6-B. Considering that NDWI-based methods find the optimal threshold using groundtruth, the result confirms the proposed method could be a better alternative way for surface water mapping.

The Orlando dataset covers a 20-km by 20-km metropolitan area. The area is dotted with hundreds of lakes and ponds over very flat terrain. As shown in Figure 7-A, lakes and ponds show various optical characteristics, which makes it challenging for image-based methods to extract accurate water bodies. However, since the proposed method exploits laser property and operates with the robust assumption that the connected water has the same elevation, it successfully extracted lakes and ponds.

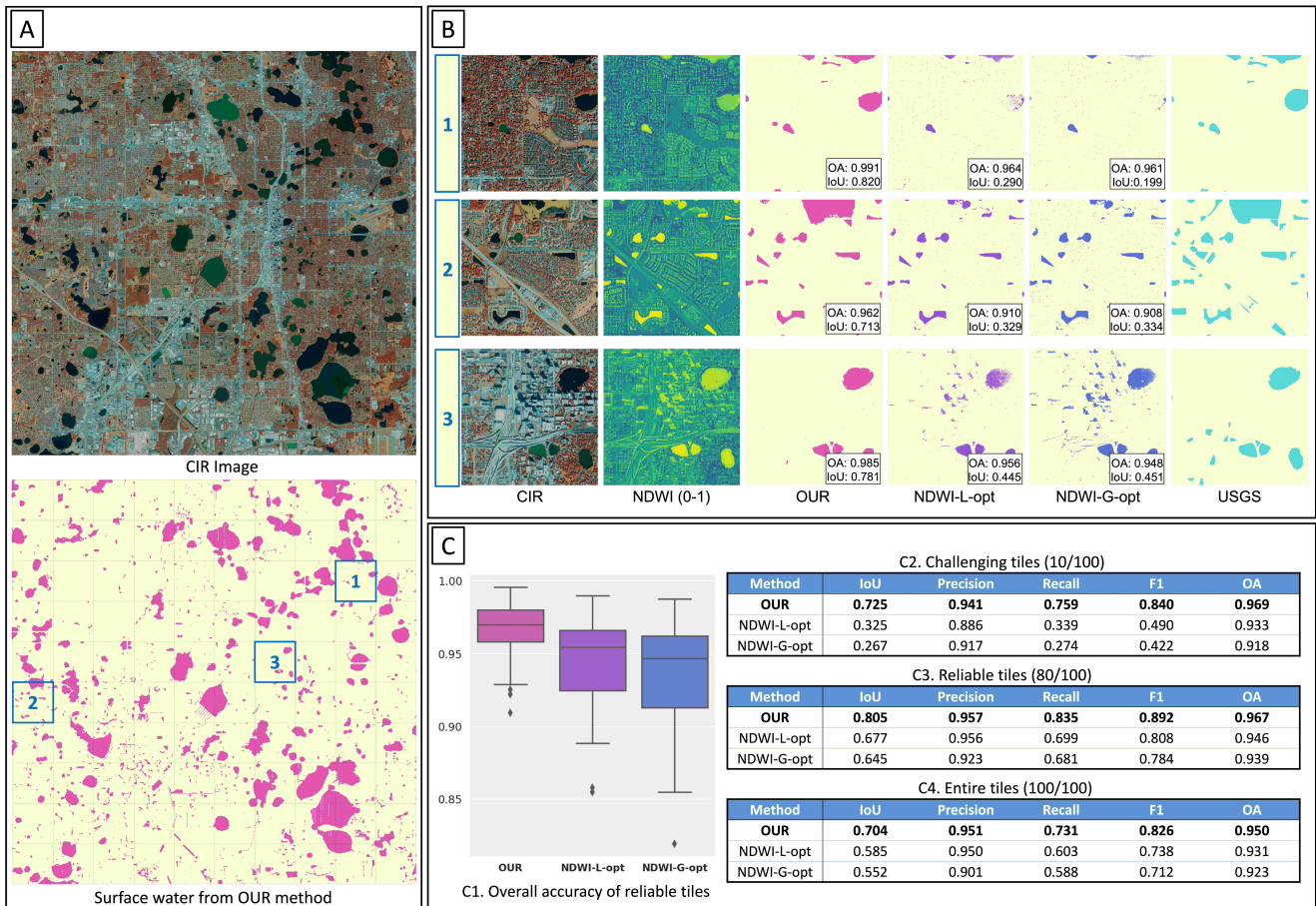


Figure 7: Results of the Orlando dataset

Figure 7-B highlighted the three sampled regions. The first row contains several small lakes and ponds in the urban area. The proposed method showed satisfactory results when compared with CIR images and USGS’s water layer, and recorded high accuracy in OA and IoU. Meanwhile, two NDWI-based methods failed to successfully extract some lakes and ponds. This is because some non-water areas have higher NDWI values than water bodies. Lowering the threshold would have allowed all the water bodies to be extracted, but that would have generated too many false positives. NDWI-L-opt detected a larger amount of water as it used a lower threshold than NDWI-G-opt, but it costs more noise in non-water areas. The second row shows a unique characteristic of the proposed method in an algae-covered lake. Unlike NDWI-based methods, the proposed method extracted the complete water body even where algae were covered. This is because algae-covered lakes still have the same level as other algae-free portions.

The third row shows the results of tiles where high-rise buildings and lakes coexist. As shown in the NDWI image, the shadows caused by high-rise buildings sometimes have higher NDWI values than the water body, resulting in many false positives in NDWI-based methods. On the other hand, since the proposed method uses a building buffer, most of the false positives could be prevented.

The proposed method also outperformed NDWI-based methods in quantitative metrics as shown in Figure 7-C. In challenging tiles, the performance gap was distinctive, especially in IoU, recall, and F1. This is because NDWI-based methods kept their thresholds low to retain overall accuracy high. A similar pattern is shown in C3 and C4 as well.

The Hollywood dataset covers a coastal urban area facing the ocean and is composed of various shapes of creeks, bays, and artificial waterways. As shown in Figure 8-A, the proposed method extracted water bodies well overall.

Figure 8-B shows a total of 3 tiles out of 10 tiles in the Hollywood dataset. Overall, both the proposed method and the two NDWI-based methods showed satisfactory performance. In all cases, OA and IoU were higher than 0.9 and 0.8, respectively. Compared to the USGS water body layer, the main errors were associated with the shadow that created by tall buildings along the coast. Otherwise, errors were either small-sized, insignificant inland water bodies or false negatives due to water transport vehicles parked along the waterway. Among different methods, the proposed method obtained the highest accuracy in both OA and IoU as it hardly generates errors from shadows or occlusions. One unique error observed in this dataset was a false negative due to the rapid current from the boat in the middle of a large water body. This is because the spectral characteristics of the wa-

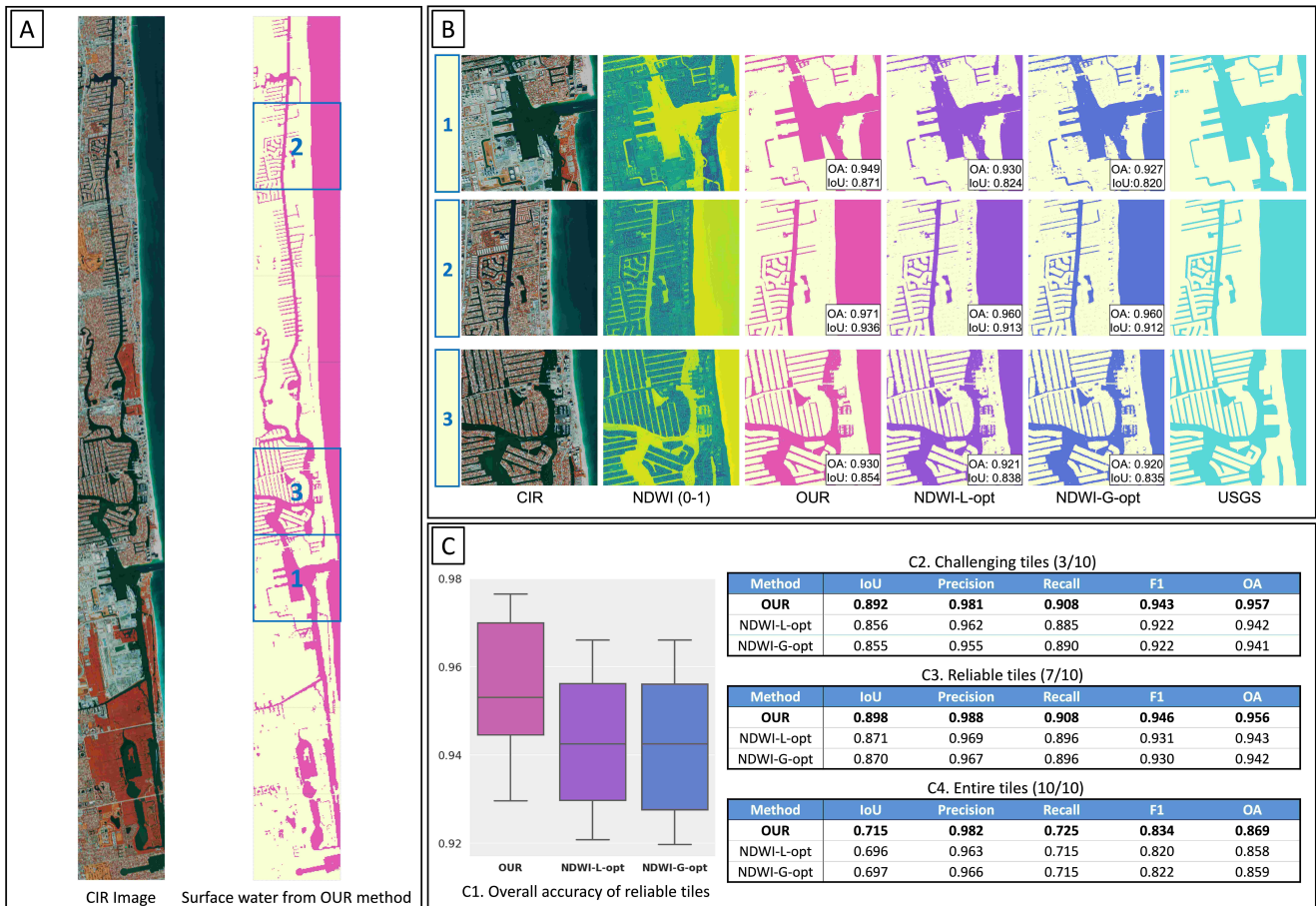


Figure 8: Results of the Hollywood dataset

ter changed temporarily due to the rapids. Although such a small size error can be easily removed by post-processing, this case confirms the advantage of the proposed method that it is hardly affected by water surface conditions.

Figure 8-C provides quantitative results. Three excluded tiles of C3 are the bottom 3 tiles as the USGS's water map classified mangroves as water bodies. Except for those three tiles, all methods showed satisfactory results, and the proposed method obtained the highest accuracy in all metrics in all cases.

6. Discussion

6.1. The impact of parameters

As confirmed by experimental results with extensive datasets with different laser scanning conditions, the proposed method can generate highly accurate surface water maps without additional parameter tuning. Additional experiments found that tuning the parameters within reasonable ranges had little effect on the overall statistics. Nevertheless, we have found that additional parameter tuning sometimes can produce more accurate results.

In this section, we provided experimental results after changing three key parameters: z-score (Z), elevational range (ER), and minimum size (MS). Z determines the confidence

interval for finding the initial water segment. For example, a Z of 1.96 represents a 95% confidence level from a standard normal distribution. The default value for Z is 2 in our method. We conducted additional experiments by changing Z to either 1.5 or 2.5. Thus, if Z is 1.5, it is expected that the method will detect water more sensitively. When Z is 2.5, the method will detect water more conservatively. ER is a small elevation interval for finding areas with the same elevation in the algorithm WERM. The default of ER is 0.1 (a range of ± 0.1 m) considering the typical vertical precision of airborne laser scanning systems. We altered the default value to either 0.05 or 0.15 so that each case extends its initial water segment more conservatively and more aggressively. Finally, the parameter MS determines the minimum size of the initial water segment to be extended to the adjacent area. To prevent insignificant bodies of water, such as puddles, from extending to the surrounding terrain, the default is set to 500 square meters. In this parameter analysis, we experimented with $100m^2$ and $1000m^2$, making the algorithm expand the initial water segment more conservatively and aggressively, respectively.

Among the entire experimental areas, we excerpted one area where the difference according to the parameters was the most prominent. Figure 9-A shows the CIR image and the surface water map generated from the proposed method

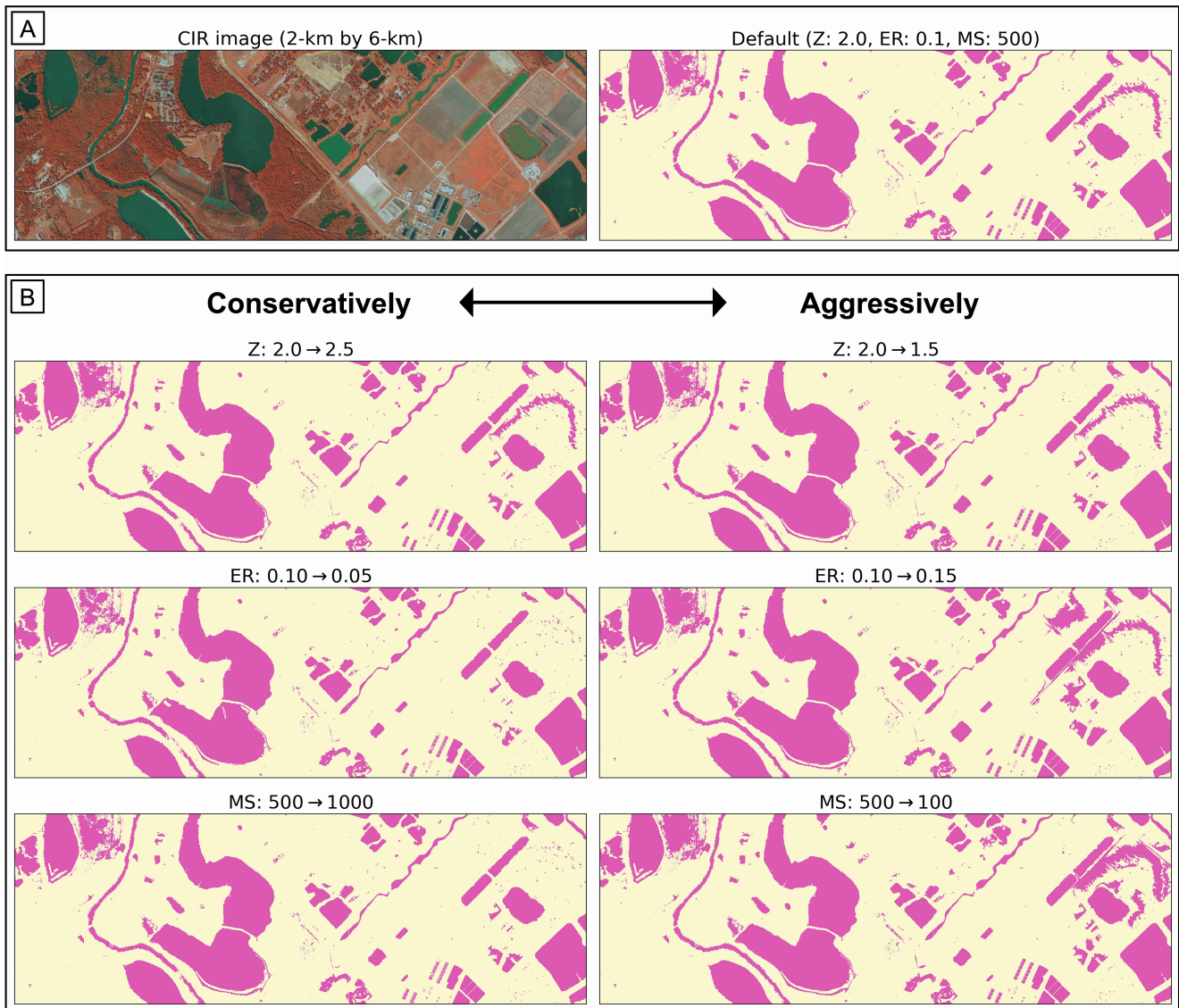


Figure 9: The impact of parameters: z-score (Z), elevation range (ER), and minimum size (MS)

with the default parameter. This area is a part of the Dallas dataset. It has the Trinity River meandering on the left and the Dallas Southside Wastewater Treatment Plant on the right. It is a very flat terrain, with a variety of water bodies, including rivers, wetlands, lakes, reservoirs, water tanks, ponds, and puddles.

Figure 9-B shows the resulting surface water map after varying three parameters' values (i.e., Z, ER, and MS). On the left side of the center, parameters are adjusted so that the water body can be extracted more conservatively, and on the right side, parameters are adjusted so that the water body can be extracted more aggressively. First, when Z was changed from the default value to 2.5 and 1.5, respectively, no significant changes occurred overall. Considering that Z works as a reference point for distinguishing water and non-water pixels using local point density, results suggest that the classification of water pixels based on the point density is quite robust. On the other hand, when the ER was changed from

the default value to 0.05 and 0.15, respectively, significant changes were observed in the resulting surface water maps. First, when ER was changed to 0.05, the error as if the small pond was flooded to the surrounding terrain on the right side of Figure 9-A was improved. On the other hand, when the ER is changed to 0.15, this "flooded" error becomes wider. A similar pattern was observed when the parameter MS was changed. When MS was set to 1000, most small ponds were not extended as they were smaller than $1,000m^2$. However, when it is set to 100, some smaller ponds were extended to adjacent terrains.

Figure 9 shows an example of how parameters can affect the resulting surface water map. The results showed that ER and MS parameters can significantly affect the resulting surface water map. However, since the two parameters are physically meaningful parameters, as they describe water level and water area, respectively, the parameter tuning and its result are quite intuitive and easy to explain. In other

words, the error and uncertainty of the proposed method can be managed relatively well compared to that of the optical image-based method.

6.2. 3D surface water map

The proposed method can generate a 3D surface water map that includes elevation information of each water body as a by-product. 2D surface water map is very useful geospatial data to support numerous studies and decision makings. However, a 2D surface water map alone cannot say where water is flowing from and where it goes. In addition, 3D information of water is helpful to monitor the water cycle or to monitor and prevent water-related pollution and disasters. Until now, most 3D hydrology has been produced by placing a 2D water layer created from optical images on a DEM. For example, the USGS commissions and distributes the production of hydro-flattened DEMs, which requires post-processing of DEM using a separate GIS layer of water. This procedure necessarily entails additional errors due to temporal difference and registration errors. With the proposed method, a full 3D topography (both terrain and water) can be produced with the same original data (Song and Jung, 2022a). We expect the proposed method can shorten complicated procedures for hydro-flattened DEM and 3D water mapping while improving their accuracies

7. Conclusion

This paper presents a surface water mapping method that provides reliable and accurate results at high resolution across a wide variety of landscapes. The proposed method uses only airborne LiDAR data based on the natural law that surface water is flat as gravity always pulls liquid molecules down. Avoiding the use of optical properties, our method enables fully automated and scalable surface water mapping. Extensive experiments with large ($\approx 2,500\text{km}^2$) and diverse landscapes (urban, coastal, and mountainous areas) confirmed that our method can generate more accurate results than NDVI-based methods even without any parameter tunings. We confirmed its overwhelming performance of water extraction in varied conditions placed in diverse environments. We confirmed its advantage, especially in steep and rugged mountains with shadows and perennial snows and complex urban environments with very small water bodies. We expect the proposed method will expedite an accurate large-scale full 3D topography mapping.

References

- S. K. Ahmad, F. Hossain, H. Eldardiry, and T. M. Pavelsky. A fusion approach for water area classification using visible, near infrared and synthetic aperture radar for south asian conditions. *IEEE Transactions on Geoscience and Remote Sensing*, 58(4):2471–2480, 2019.
- C. Arrighi and L. Campo. Effects of digital terrain model uncertainties on high-resolution urban flood damage assessment. *Journal of Flood Risk Management*, 12(S2):e12530, 2019.
- R. H. Becker, M. Sayers, D. Dehm, R. Shuchman, K. Quintero, K. Bosse, and R. Sawtell. Unmanned aerial system based spectroradiometer for monitoring harmful algal blooms: A new paradigm in water quality monitoring. *Journal of Great Lakes Research*, 45(3):444–453, 2019.
- J. Biggs, S. Von Fumetti, and M. Kelly-Quinn. The importance of small waterbodies for biodiversity and ecosystem services: implications for policy makers. *Hydrobiologia*, 793(1):3–39, 2017.
- A. Brzank, C. Heipke, J. Goepfert, and U. Soergel. Aspects of generating precise digital terrain models in the wadden sea from lidar–water classification and structure line extraction. *ISPRS Journal of Photogrammetry and Remote Sensing*, 63(5):510–528, 2008.
- K. Cawse-Nicholson, P. A. Townsend, D. Schimel, A. M. Assiri, P. L. Blake, M. F. Buongiorno, P. Campbell, N. Carmon, K. A. Casey, R. E. Correa-Pabón, et al. Nasa’s surface biology and geology designated observable: A perspective on surface imaging algorithms. *Remote Sensing of Environment*, 257:112349, 2021.
- Y. Chen, L. Tang, Z. Kan, M. Bilal, and Q. Li. A novel water body extraction neural network (wbe-nn) for optical high-resolution multispectral imagery. *Journal of Hydrology*, 588:125092, 2020.
- N. Crasto, C. Hopkinson, D. Forbes, L. Lesack, P. Marsh, I. Spooner, and J. Van Der Sanden. A lidar-based decision-tree classification of open water surfaces in an arctic delta. *Remote Sensing of Environment*, 164:90–102, 2015.
- Y. Dong, L. Fan, J. Zhao, S. Huang, C. Geiß, L. Wang, and H. Taubenböck. Mapping of small water bodies with integrated spatial information for time series images of optical remote sensing. *Journal of Hydrology*, 614:128580, 2022.
- G. L. Feyisa, H. Meilby, R. Fensholt, and S. R. Proud. Automated water extraction index: A new technique for surface water mapping using landsat imagery. *Remote Sensing of Environment*, 140:23–35, 2014.
- M. Flörke, C. Schneider, and R. I. McDonald. Water competition between cities and agriculture driven by climate change and urban growth. *Nature Sustainability*, 1(1):51–58, 2018.
- A. Y. Hoekstra, J. Buurman, and K. C. Van Ginkel. Urban water security: A review. *Environmental research letters*, 13(5):053002, 2018.
- B. Höfle, M. Vetter, N. Pfeifer, G. Mandlbürger, and J. Stötter. Water surface mapping from airborne laser scanning using signal intensity and elevation data. *Earth Surface Processes and Landforms*, 34(12):1635–1649, 2009.
- C. Huang, Y. Chen, S. Zhang, and J. Wu. Detecting, extracting, and monitoring surface water from space using optical sensors: A review. *Reviews of Geophysics*, 56(2):333–360, 2018.
- F. Isikdogan, A. C. Bovik, and P. Passalacqua. Surface water mapping by deep learning. *IEEE journal of selected topics in applied earth observations and remote sensing*, 10(11):4909–4918, 2017.
- A. A. Jarihani, J. N. Callow, T. R. McVicar, T. G. Van Niel, and J. R. Larsen. Satellite-derived digital elevation model (dem) selection, preparation and correction for hydrodynamic modelling in large, low-gradient and data-sparse catchments. *Journal of Hydrology*, 524:489–506, 2015.
- L. Ji, L. Zhang, and B. Wylie. Analysis of dynamic thresholds for the normalized difference water index. *Photogrammetric Engineering & Remote Sensing*, 75(11):1307–1317, 2009.
- M. Kelly-Quinn, J. Biggs, S. Brooks, P. Fortuño, S. Hegarty, J. Jones, and F. Regan. Opportunities, approaches and challenges to the engagement of citizens in filling small water body data gaps. *Hydrobiologia*, pages 1–21, 2022.
- A. Khandelwal, A. Karpatne, M. E. Marlier, J. Kim, D. P. Lettenmaier, and V. Kumar. An approach for global monitoring of surface water extent variations in reservoirs using modis data. *Remote sensing of Environment*, 202:113–128, 2017.
- W. Kim, J.-E. Moon, Y.-J. Park, and J. Ishizaka. Evaluation of chlorophyll retrievals from geostationary ocean color imager (goci) for the north-east asian region. *Remote Sensing of Environment*, 184:482–495, 2016.
- B. C. Ko, H. H. Kim, and J. Y. Nam. Classification of potential water bodies using landsat 8 oli and a combination of two boosted random forest classifiers. *Sensors*, 15(6):13763–13777, 2015.
- H. Liu, P. Gong, J. Wang, X. Wang, G. Ning, and B. Xu. Production of global daily seamless data cubes and quantification of global land cover change from 1985 to 2020-imap world 1.0. *Remote Sensing of Environment*, 258:112364, 2021.
- R. Malinowski, B. Höfle, K. Koenig, G. Groom, W. Schwanghart, and G. Heckrath. Local-scale flood mapping on vegetated floodplains from

- radiometrically calibrated airborne lidar data. *ISPRS Journal of Photogrammetry and Remote Sensing*, 119:267–279, 2016.
- W. Mao, K. Yang, W. Zhang, Y. Wang, and M. Li. High-resolution global water body datasets underestimate the extent of small rivers. *International Journal of Remote Sensing*, 43(11):4315–4330, 2022.
- V. S. Martins, C. C. F. Barbosa, L. A. S. De Carvalho, D. S. F. Jorge, F. d. L. Lobo, and E. M. L. d. M. Novo. Assessment of atmospheric correction methods for sentinel-2 msi images applied to amazon floodplain lakes. *Remote Sensing*, 9(4):322, 2017.
- R. B. Moore and T. G. Dewald. The road to nhdp lus—advancements in digital stream networks and associated catchments. *JAWRA Journal of the American Water Resources Association*, 52(4):890–900, 2016.
- R. B. Moore, L. D. McKay, A. H. Rea, T. R. Bondelid, C. V. Price, T. G. Dewald, C. M. Johnston, et al. User’s guide for the national hydrography dataset plus (nhdplus) high resolution. *Open-File Report-US Geological Survey*, (2019-1096), 2019.
- J. G. Moreno-Torres, T. Raeder, R. Alaiz-Rodríguez, N. V. Chawla, and F. Herrera. A unifying view on dataset shift in classification. *Pattern recognition*, 45(1):521–530, 2012.
- N. J. Murray, S. P. Phinn, R. A. Fuller, M. DeWitt, R. Ferrari, R. Johnston, N. Clinton, and M. B. Lyons. High-resolution global maps of tidal flat ecosystems from 1984 to 2019. *Scientific Data*, 9(1):1–9, 2022.
- Z. Musa, I. Popescu, and A. Mynett. A review of applications of satellite sar, optical, altimetry and dem data for surface water modelling, mapping and parameter estimation. *Hydrology and Earth System Sciences*, 19(9):3755–3769, 2015.
- D. Odermatt, A. Gitelson, V. E. Brando, and M. Schaepman. Review of constituent retrieval in optically deep and complex waters from satellite imagery. *Remote sensing of environment*, 118:116–126, 2012.
- A. Ogilvie, G. Belaud, S. Massuel, M. Mulligan, P. Le Goulven, and R. Calvez. Surface water monitoring in small water bodies: Potential and limits of multi-sensor landsat time series. *Hydrology and Earth System Sciences*, 22(8):4349–4380, 2018.
- J.-F. Pekel, A. Cottam, N. Gorelick, and A. S. Belward. High-resolution mapping of global surface water and its long-term changes. *Nature*, 540(7633):418–422, 2016.
- A. H. Pickens, M. C. Hansen, M. Hancher, S. V. Stehman, A. Tyukavina, P. Potapov, B. Marroquin, and Z. Sherani. Mapping and sampling to characterize global inland water dynamics from 1999 to 2018 with full landsat time-series. *Remote Sensing of Environment*, 243:111792, 2020.
- N. L. Poff, C. M. Brown, T. E. Grantham, J. H. Matthews, M. A. Palmer, C. M. Spence, R. L. Wilby, M. Haasnoot, G. F. Mendoza, K. C. Dominique, et al. Sustainable water management under future uncertainty with eco-engineering decision scaling. *Nature Climate Change*, 6(1):25–34, 2016.
- N. Qayyum, S. Ghuffar, H. M. Ahmad, A. Yousaf, and I. Shahid. Glacial lakes mapping using multi satellite planetscope imagery and deep learning. *ISPRS International Journal of Geo-Information*, 9(10):560, 2020.
- W. D. Riley, E. C. Potter, J. Biggs, A. L. Collins, H. P. Jarvie, J. I. Jones, M. Kelly-Quinn, S. J. Ormerod, D. A. Sear, R. L. Wilby, et al. Small water bodies in great britain and ireland: Ecosystem function, human-generated degradation, and options for restorative action. *Science of the Total Environment*, 645:1598–1616, 2018.
- C. Robinson, L. Hou, K. Malkin, R. Soobitsky, J. Czawlytko, B. Dilkina, and N. Jovic. Large scale high-resolution land cover mapping with multi-resolution data. In *Proceedings of the IEEE/CVF Conference on Computer Vision and Pattern Recognition*, pages 12726–12735, 2019.
- B. F. Sanders, J. E. Schubert, D. T. Kahl, K. J. Mach, D. Brady, A. AghaKouchak, F. Forman, R. A. Matthew, N. Ulibarri, and S. J. Davis. Large and inequitable flood risks in los angeles, california. *Nature sustainability*, pages 1–11, 2022.
- A. Shaker, W. Y. Yan, and P. E. LaRocque. Automatic land-water classification using multispectral airborne lidar data for near-shore and river environments. *ISPRS journal of photogrammetry and remote sensing*, 152:94–108, 2019.
- J. Smeckaert, C. Mallet, N. David, N. Chehata, and A. Ferraz. Large-scale classification of water areas using airborne topographic lidar data. *Remote sensing of environment*, 138:134–148, 2013.
- P. Sogno, I. Klein, and C. Kuenzer. Remote sensing of surface water dynamics in the context of global change—a review. *Remote Sensing*, 14(10):2475, 2022.
- H. Song and J. Jung. An object-based ground filtering of airborne lidar data for dtm generation. *arXiv preprint arXiv:2208.11243*, 2022a.
- H. Song and J. Jung. An unsupervised, open-source workflow for 2d and 3d building mapping from airborne lidar data. *arXiv preprint arXiv:2205.14585*, 2022b.
- H. Song, Y. Kim, and Y. Kim. A patch-based light convolutional neural network for land-cover mapping using landsat-8 images. *Remote Sensing*, 11(2):114, 2019.
- J. Stoker and B. Miller. The accuracy and consistency of 3d elevation program data: A systematic analysis. *Remote Sensing*, 14(4):940, 2022.
- E. Straffellini, S. Cucchiario, and P. Tarolli. Mapping potential surface ponding in agriculture using uav-sfm. *Earth Surface Processes and Landforms*, 46(10):1926–1940, 2021.
- X. Sun, L. Li, B. Zhang, D. Chen, and L. Gao. Soft urban water cover extraction using mixed training samples and support vector machines. *International Journal of Remote Sensing*, 36(13):3331–3344, 2015.
- D. Viviroli, D. R. Archer, W. Buytaert, H. J. Fowler, G. B. Greenwood, A. F. Hamlet, Y. Huang, G. Koboltschnig, M. Litaor, J. I. López-Moreno, et al. Climate change and mountain water resources: overview and recommendations for research, management and policy. *Hydrology and Earth System Sciences*, 15(2):471–504, 2011.
- Y. Wang, Z. Li, C. Zeng, G.-S. Xia, and H. Shen. An urban water extraction method combining deep learning and google earth engine. *IEEE Journal of Selected Topics in Applied Earth Observations and Remote Sensing*, 13:769–782, 2020.
- W. Wu, H. Qi, Z. Rong, L. Liu, and H. Su. Scribble-supervised segmentation of aerial building footprints using adversarial learning. *IEEE Access*, 6:58898–58911, 2018.
- H. Xu. Modification of normalised difference water index (ndwi) to enhance open water features in remotely sensed imagery. *International journal of remote sensing*, 27(14):3025–3033, 2006.
- P. Xu, M. Herold, N.-E. Tsombazar, and J. G. Clevers. Towards a comprehensive and consistent global aquatic land cover characterization framework addressing multiple user needs. *Remote Sensing of Environment*, 250:112034, 2020.
- D. Yamazaki, M. A. Trigg, and D. Ikeshima. Development of a global 90 m water body map using multi-temporal landsat images. *Remote Sensing of Environment*, 171:337–351, 2015.
- W. Y. Yan, A. Shaker, and P. E. LaRocque. Scan line intensity-elevation ratio (slier): An airborne lidar ratio index for automatic water surface mapping. *Remote Sensing*, 11(7):814, 2019.
- X. Yang, Q. Qin, P. Grussenmeyer, and M. Koehl. Urban surface water body detection with suppressed built-up noise based on water indices from sentinel-2 msi imagery. *Remote sensing of environment*, 219:259–270, 2018.
- Y. Zhang, G. Chen, S. W. Myint, Y. Zhou, G. J. Hay, J. Vukomanovic, and R. K. Meentemeyer. Urbanwatch: A 1-meter resolution land cover and land use database for 22 major cities in the united states. *Remote Sensing of Environment*, 278:113106, 2022.